ECRONICON OPEN ACCESS

EC ORTHOPAEDICS
Research Article

Effectiveness of Purmorphamine Loaded Biodegradable 3D Polylactic Acid/Polycaprolactone/Hydroxyapatite Scaffold in a Critical-Sized Radial Bone Defect in Rat

Ahmad Oryan[1]*, Shadi Hassanajili[2] and Sonia Sahvieh[1]

[1]*Department of Pathology, School of Veterinary Medicine, Shiraz University, Shiraz, Iran*

[2]*Department of Chemical Engineering, School of Chemical and Petroleum Engineering, Shiraz University, Shiraz, Iran*

***Corresponding Author:** Ahmad Oryan, Department of Pathology, School of Veterinary Medicine, Shiraz University, Shiraz, Iran.

Received: May 09, 2022 ; Published: May 24, 2022

Abstract

A critical bone defect is an important problem that needs the intervention of regenerative medicine and tissue engineering to increase its healing quality at a minimum time. The polylactic acid (PLA)/polycaprolactone (PCL)/hydroxyapatite (HA) scaffold was loaded for the first time by purmorphamine (PMA), as an osteoinductive drug, and the drug delivery effect of the scaffold was tested on radius bone healing in rat. The scanning ultramicrographs, X-ray diffraction, rheology, and Fourier transform-infrared spectroscopy were used to study the scaffold features. Forty Wistar rats were divided into the following four groups (n = 10 in each group): the defect in the first group was left empty (control), and the defect of the 2nd to the 4th groups was filled by autograft, scaffold, and the PMA-loaded scaffold respectively. The level of OPN, OC, and CD31 expression was higher in the scaffold and PMA-loaded scaffold groups than the control group in the qRT-PCR ($P < 0.05$). The radiology, computed tomography scan, immunohistochemical, biomechanical, and histomorphometric investigations depicted a significant improvement in the PMA-loaded scaffold in comparison to the empty defect ($P < 0.05$). Therefore, the scaffold showed a significant influence compared to the control group ($P < 0.05$), and PMA promoted the potential of the PCL/PLA/HA scaffold on bone regeneration.

Keywords: *PLA/PCL/HA Scaffold; Purmorphamine; Bone Regeneration; Radius Bone; Rat*

Introduction

Bone regulates hormones, stores minerals, produces blood cells, and supports and protects other organs. Bone diseases such as bone cancer, osteoporosis (OP), osteoarthritis (OA), chronic bone infections, osteomyelitis, myeloma-related bone diseases, and some other problems, including osteotomies, non-union bone defects, trauma and pathologic fractures which damage bone tissue are the most significant challenges for orthopedic surgeons [1-5]. A proper and successful fracture healing would occur when the new bone formation remodels through osteoclasts and organizes a new vasculature formation with adequate stability. Ultimately, the new bone tissue obtains the skeletal function [6,7].

In critical defects, the ability of bone tissue to regenerate itself is limited, and it is necessary to find a new approach to solve the difficulties. Tissue engineering is an appropriate method in regenerative medicine. Different types of natural materials such as alginate, collagen, fibrin, chitin, gelatin, chitosan, hyaluronic acid, and glycosaminoglycan (GAGs) and several synthetic biomaterials including polycaprolactone (PCL), polylactic acid (PLA), polyfumarates, polyglycolic acid (PGA) and copolymers of PGA and PLA (PLGA) have been used as bone implants [1,8-11]. Combination of various types of scaffold loaded with drugs, growth factors, bioactive molecules, and cells has been

applied in reconstructive, orthopedic, and plastic surgeries [1,10,12-15]. Bone substitutes should have some favorable healing characteristics such as osteoinduction (induction of undifferentiated cells to osteoblasts and osteocytes), osteogenesis (differentiation of osteoprogenitor cells to induce a new bone tissue) and osteoconduction (to establish a suitable term to osteoprogenitor cells and osteoblasts adherence) to support osteoregeneration [16].

Biodegradability, controllable pore sizes, non-toxicity, biocompatibility, and osteogenic ability are some features that a bone scaffold should have to enhance new bone formation [17,18]. Ca_{10} $(PO_4)_6$ $(OH)_2$ is the formula of hydroxyapatite (HA), which shows that it has a composition like bone tissue. New bone formation would be initiated by HA because of its proper porosity that permits cells to proliferate, attach, and differentiate [16]. Biodegrading to non-toxic ingredients and biocompatibility are the main features of PLA and PCL; however, there are some problems with each of these polymers that limits their application as bone implants. PLA is a fast degradable polymer and is more brittle than PCL; however, cell adhesion on the pure PCL composite is better. It has been shown that the PCL/PLA scaffold has a suitable effect on stem cells to be differentiated to the osteogenic cells [19]. In fact, by adding HA to the PCL/PLA scaffold, the differentiation and proliferation degree of the osteogenic cells enhances to result in excess new bone formation [17,20-22]. The study hypothesis was to investigate the potential of PLA/PCL/HA scaffold on bone regeneration and its comparison after loading with purmorphamine as an osteoinductive drug.

2,6,9-Trisubstituted purine called purmorphamine (PMA) is a hedgehog agonist that enhances the differentiation of osteogenic cells from the preosteoblasts (MC3T3-E1), human mesenchymal cells (hMSCs) and embryonic fibroblasts of mouse (C3H10T1/2) and also up-regulates the core-binding factor alpha 1 (Cbfa1) (the factor of osteoblast transcription) [23-25]. This drug inhibits the transmembrane protein [Smoothened (SMO)] and results in osteoinductivity due to an increase in the hedgehog (Hh) signaling [26,27]. Hh signaling is activated with PMA and culminates the increase of transcription of protein patched (Ptch), alkaline phosphatase (ALP), and glioma-associated oncogene homolog 1 (Gli1) and induces the differentiation of bone marrow mesenchymal stem cells and human multipotent adipose-derived stem cells to osteoblasts [24,28]. It has been shown that 3 μM of PMA exerted an enhanced effect on the human BMSCs to differentiate to the osteogenic cells (*in vitro* and *in vivo*) [29]. PMA induced the activity of alkaline phosphatase via up-regulation, runt-related transcription factor 2 (RUNX-2) expression, and osteocalcin (OC) up-regulation [24,29]. It has been stated that PMA at 1, 2, and 3 μM doses does not increase cell viability and cell proliferation, but it enhances ALP activity. It has also been stated that differentiation of osteoblasts is enhanced by PMA and ultimately results in the formation of bone-like nodules [30]. PMA could promote bone regeneration by enhanced differentiation of stem cells to osteoblasts. Bahrami and colleagues stated that the capacity of differentiation of the human endometrial stem cells to osteoblasts and osteoid formation was increased when PMA was loaded on the collagen/HA scaffold [31].

The potential of PLA/PCL/HA scaffold that was fabricated by freeze-drying and indirect three dimensional (3D) printing methods on bone healing was evaluated by *in vitro* and *in vivo* studies. Biodegradability, osteoblasts viability, mechanical behavior, calcium deposition, and physical features of this scaffold were estimated. We investigated the regeneration potential of PMA after loading on the scaffold and compared it to the autograft as the golden treatment. The effects of different treatment strategies on bone healing were evaluated by gross morphological, histopathological, histomorphometrical, immunohistochemical (IHC), biomechanical, radiological, and computed tomography (CT) scan examinations.

Materials and Methods

Fabrication of the scaffold

The SOLIDWORKS software was used in designing the mold to fabricate the scaffold and the mold included the 5 × 5 × 5 mm cubic-shaped struts. The indirect 3D printer (ZMorph Co.) was used for scaffold fabrication by polylactic acid (MG Chemicals), polycaprolactone (Sigma Aldrich), and hydroxyapatite (Merck Co.). Poly (vinyl alcohol) filament was used to print the negative mold. All the materials were

dried with a vacuum oven (24 h), and the 10% w/v PLA and PCL were added to 99.8% chloroform (Merck Co.), respectively, and stirred for 1 h to dissolve. Fructose (Merck Co.) was added to the solution, then HA was incorporated after 1 h. The later suspension was spilled into the negative mold slowly and left at -80 °C until the elimination of the solvent.

Accomplished tests on the scaffold

Complex viscosity and dynamic functions (0.5 - 100 rad/s, 220 °C) were measured by a rheometer purchased from Anton Paar, Austria (Physica MCR 302) to find the PLA, PCL/PLA blend, and PCL rheological behavior [32]. The presence of HA was estimated by elemental analysis, using energy-dispersive X-ray spectroscopy (EDS). The microstructure and diameter of the pores of the scaffold in the scanning electron ultramicrographs (SEM) (TESCAN-Vega 3 SEM system) were measured by Image J software. Although, the cell morphology and attachment on the scaffold were determined after 24 hours of cell seeding via SEM images. The cells (6×10^3) were seeded on the PLA/PCL/HA scaffold. The neutral red test (0.0005% neutral red in normal saline) was performed to detect cell viability at days 3, 7, and 10 post-seeding. All blocks were washed by normal saline and were then fixed with calcium formol. Acid alcohol was utilized as the elution (optic density of the eluted dye = 550 nm wavelength).

The stress-strain diagram of the mechanical performance was established by the compression test done on the PLA/PCL/HA scaffold. The Zwick/roell apparatus compressed a cubic of the scaffold by 1 mm/min speed. The fluid replacement test was done on the scaffold to understand its porosity. It was performed by the ethanol soaked pores of the scaffold and the porosity was measured by the following formula [33]:

$[v_1$ (volume of ethanol) - v_3 (the rest of the ethanol volume after scaffold removal)] + [v_2 (volume of the scaffold and ethanol) - v_1] = v

Porosity = $v_1 - v_3 / v \times 100$

The degradation behavior was determined by PBS at 7, 14, 21, 28, and 35 days (37 °C) by the below equation: (W_1 = degraded sample, W_2 = the elemental sample)

Mass loss = $(W_1 - W_2)/W_1$

The samples were transferred to a vacuum oven (for 24 h), and the pH value was estimated after removing the PBS solution from the samples. The Bruker D8 advance apparatus was performed on the PCL, PLA, and HA for the X-ray diffraction (XRD) test at 25 °C in a 2θ range of 10-80° [34]. Identification of the molecular interaction was obtained from the Fourier transform infrared (FTIR) analysis (NEXUS670) [35].

Loading the scaffold by PMA

Based on the Faghihi and colleagues' experiment, 3 µM dosage of PMA (SML0868, Sigma) was loaded on the PLA/PCL/HA scaffold (sterilized by 70% ethanol and UV light) [29].

Quantitative real-time polymerase chain reaction (qRT-PCR) analysis

The potential of PLA/PCL/HA scaffold in inducing osteogenesis was determined based on measuring the OPN and OCN markers and angiogenesis (CD31 marker) by qRT-PCR on day 21. The human umbilical cord mesenchymal stem cells were supplied from the Cell Therapy Center at Royan Institute. The whole RNA was collected from the cells, using the RNeasy Micro Kit (Qiagen-74004). The synthesized cDNA was then done with the Revert Aid First Strand cDNA Synthesis Kit (Fermentas, Sankt Leon-Rot, Germany, k1632). SYBR® Green PCR Master Mix (Applied Biosystems Life Technologies, REF 4367659) was used to duplicate the qRT-PCR reaction with the real-

time PCR system (Applied Biosystems Life Technologies, ABiStepOnePlus). The results were analyzed by the StepOne software (Applied Biosystems, version 2.1) at last. A comparative CT method or 2-ΔΔCt method was utilized to quantify gene expression, where some target genes normalized to calibrator group (2d cell culture flask) and endogenous control (GAPDH).

In vivo study

Forty male adult Wistar rats (225 ± 25g) were divided into four groups [1. Control (empty defect) 2. autograft 3. Scaffold (implanted on the defect region) 4. PMA loaded scaffold] (n = 10 in each group). The animals were housed in 59 × 38.5 × 30 cm cages in groups of four and for acclimatization they were housed five days before the start of study [(humidity = 30-70%, temperature = 19°C - 26°, lighting = 300 lux, 12:12 light:dark cycle), with rat maintenance food and water *ad libitum*]. All animals were monitored at the moment of housing twice daily for health status and no adverse event was seen. The rats were generally anesthetized, using ketamine hydrochloride (20 mg/kg) and 2 mg/kg xylazine, intramuscularly. A 3-cm incision was made in the skin to access the radial bone; the bone was then osteotomized bilaterally by an electrical bone saw (Strong, Seoul, South Korea) to create a 5-mm defect. Antibiotic therapy and post-operative analgesia were continued for 3 days by enrofloxacin (Irfan, Iran) and meloxicam (Razak, Iran), subcutaneously.

Gross pathology

Macroscopic evaluation was based on scoring the capacity of bone healing at the defect region as follows:

0 = non-union defects

+1 = incomplete union (fibrous connective tissue)

+2 = incomplete union (cartilage tissue)

3 = complete union (bridging bone) [36].

Radiologic and CT-scan analysis

Radiographic measurement was done from the lateral surface of the radius bone in all animals under general anesthesia at the 40^{th} and 80^{th} days post-surgery. CT scan was performed on the forelimbs to estimate the rate of gap closure based upon the X direction depicted cranial/caudal, Y direction, dorsoventral, and Z direction, lateral/medial of the radius. The percentage of gap closure (%) was obtained from the digital radiograph analysis.

Histopathology and histomorphometry

The bone samples were fixed in neutral buffer formalin and then decalcified by 10% EDTA for 35 days. The samples were processed and embedded in paraffin wax to make 5 µm sections and then stained by hematoxylin and eosin (H and E). The fibroblasts, fibrocytes, chondroblasts, chondrocytes, osteoblasts, osteocytes, and inflammatory cells in the wound bed were counted. The proportion of fibrous connective tissue or collagen density, new cartilage formation, bone ingrowth, and number of blood vessels were also evaluated (Image-Pro Plus V.6 software, magnification × 400).

Immunohistochemical (IHC) analysis

CD31 (ab119339, Abcam, MA) and osteocalcin (ab13420, Abcam, MA) were estimated in the samples from the defect region. The samples were left in 60 °C citrate buffer solution overnight and then blocked by hydrogen peroxide/methanol. The 3,3'-diaminobenzidine developed the color reaction and then counterstained with hematoxylin.

Biomechanical analysis

The whole forelimbs of all rats (n = 5 per group) were collected after day 80 post-operation and wrapped in moist gauzes and kept at -20 °C. Each sample was settled on two supporting bars (16 mm distance) and the last bar was under midline of the defect region for the 3-point bending test [37]. All samples were loaded at the 5 mm/min strain rate until the samples were fractured. The load-deformation diagram (universal testing machine, Instron, London, UK) was drawn and the maximum load, stiffness, strain, and maximum stress were analyzed.

Statistical analysis

One-way analysis of variance (Tukey *post hoc*) analyzed the quantitative data, and Kruskal-Wallis analyzed the qualitative data and when $P < 0.05$ Mann-Whitney *U-test* was used.

Results

Scaffold features

The SEM ultramicrographs showed that the PLA/PCL/HA scaffold had suitable interconnectivity with sufficient macro- and micro-pores. The average diameter of the micropores was 141.0 ± 47.0 µm, and the thickness of pore walls was 27.9 ± 2.2 µm [Figure 1(A)]. The cells were attached strongly to the PLA/PCL/HA scaffold after 24 hours post-seeding by their pseudopodia [Figure 1(A)]. The mean porosity (%) of the scaffold was measured around 69-71%.

The EDS results are depicted in table 1 to reveal the elemental analysis (Ca, C, O, and P appearance on the scaffold surface). The weight ratio of Ca/P was 1.7. The rheology results of PCL, PCL/PLA (50/50), and PLA were displayed by the diagram of the complex viscosity curve versus the angular frequency [Figure 1(B)]. Micro-pores, polymers degradation, and porosity are the factors that determine the degradation rate of the scaffold. As shown in table 2, the PLA/PCL/HA scaffold demonstrated a lower degradation rate compared to PCL and the highest degradation rate belonged to the PLA portion. As much as 2 - 2.5% of the scaffold was degraded in the neutral pH after 35 days, which provided a good situation for osteoblasts and osteocytes to migrate to the defect region before complete degradation of this scaffold. The stress-strain diagram of the scaffold is shown in figure 1(C) (compressive modulus (MPa): 0.6339 ± 0.03995). The linear behavior of the curve was observed until 20% of the strain and the slope of the diagram was at 20 - 45% of the strain. This slope revealed that the scaffold pores densified and then thoroughly collapsed after 45% strain. The cell viability after 3, 7, and 10 days by neutral red test is depicted in table 3.

Element %	C	O	Ca	P
50/50 - 35%	48.5 ± 2.3	34.4 ± 4.7	10.4 ± 0.1	6.7 ± 1

Table 1: *Elemental analysis of the scaffold.*

	Mean ± SD
7 days	101.2291 ± 0.116372
14 days	100.7574 ± 0.002957
21 days	99.48005 ± 0.001224
28 days	98.72202 ± 0.003591
35 days	97.83563 ± 0.491151

Table 2: *Degradation rate of the scaffold at 7, 14, 21, 28, and 35 days SD, standard deviation.*

	Mean ± SD	
Cells (neutral red)	3 days	1.29425 ± 0.13000
	7 days	1.28600 ± 0.23200
	10 days	1.51275 ± 0.17500

Table 3: *Cell number of the scaffold SD, standard deviation.*

Table 4 shows that the HA particles resulted in pH alteration and an increase in the pH value was due to the release of alkaline ions from the HA particles into the solution and the decrease in the pH value was due to releasing of the acidic by-products into the solution from the polymers. The crystallinity of PCL was higher than PLA and the PLA/PCL/HA was greater than PCL/PLA, which was probably because of the interaction between HA and PLA. The results of FTIR spectroscopy showed in Fig. 1(D). The peak positions of each pure material are depicted in table 5 and the diagram demonstrates some shifts of peaks of the HA, PCL, PCL/PLA/HA, and PLA bands (e.g., carbonyl and hydroxyl groups). The crystallinity of HA with the peaks at 26˚, 31.8˚, 32.9˚, 40˚ and 49˚ and lattice parameters at a = 0.943 nm, b = 0.493 nm and c=0.688 nm, PLA with the peaks at 2θ = 16.6˚, 2θ = 18.9˚, PCL with the peaks at 2θ = 21.6˚, 2θ = 23.8˚ and lattice parameters of both PCL and PLA at a=0.948 nm, b = 0.498 nm and c = 1.727 nm is displayed with the XRD graph in Figure 1(E).

	Mean ± SD
7 days	7.606667 ± 0.025166
14 days	7.633333 ± 0.031316
21 days	7.576667 ± 0.025166
28 days	7.573333 ± 0.023094
35 days	7.543333 ± 0.030415

Table 4: *The pH changes at 7, 14, 21, 28, and 35 days SD, standard deviation.*

	CH_2 Symmetric Stretch	Asymmetric Stretch	Carbonyl Stretch	C-O Stretch	CH_3 Stretch	PO_4^{-3} Stretch	OH Stretch
PCL	2940 cm^{-1}	2860 cm^{-1}	1720 cm^{-1}	Around 1160 cm^{-1}			
PLA			1740 cm^{-1}	1032 cm^{-1}	2883 cm^{-1}		
HA						Around 1036 cm^{-1}	3500 cm^{-1}

Table 5: *FTIR data of samples.*

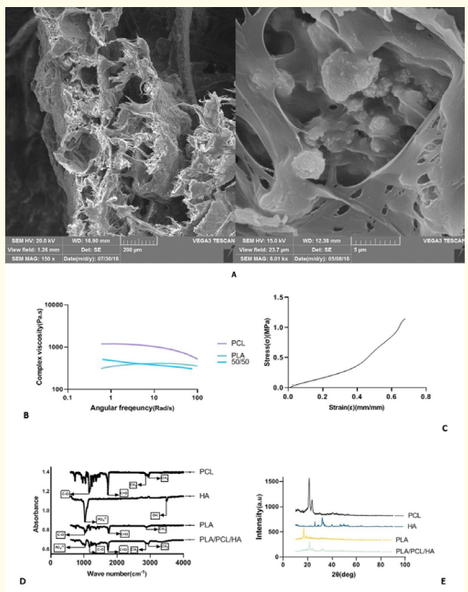

Figure 1: *A: Ultramicrograph of the PLA/PCL/HA scaffold. B: The complex viscosity variation to the angular frequency. C: Stress-strain diagram. D: FTIR diagram of the PCL/PLA/HA, HA, PCL, and PLA nanopowder. E: XRD patterns of the PLA/PCL/HA, PLA, PCL scaffolds and HA nanopowder.*

qRT-PCR analysis

qRT-PCR showed the level of osteogenic and angiogenic-related gene expressions after 21 days post-seeding (Figure 2). The PMA-loaded scaffold depicted a significantly higher expression level of angiogenic marker (CD31) compared to the control group (2D-cell culture) (*P < 0.05*). The expression level of osteogenic markers (OPN and OCN) also increased in the scaffold and PMA-loaded scaffold groups when compared to the control group (*P < 0.01)* but the highest level of osteogenic markers was related to the PMA-loaded scaffold.

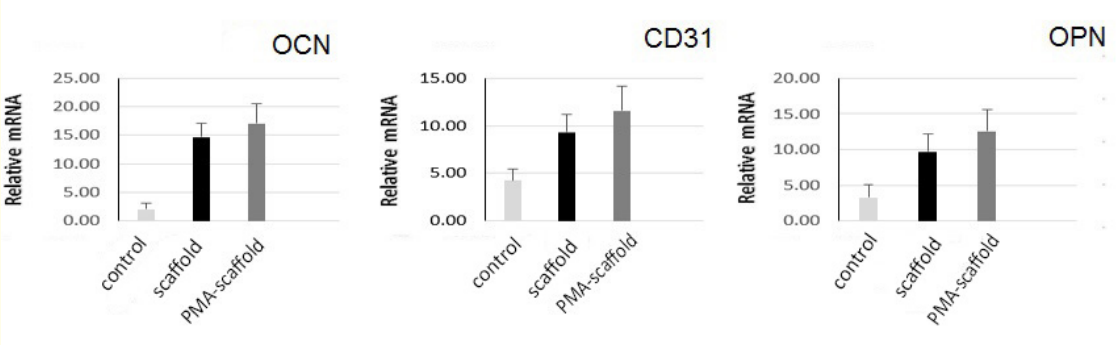

Figure 2: *Expression level of the OPN, CD31, and OCN genes that were analyzed with qRT-PCR on day 21. The expression level of all genes were increased in the scaffold group in comparison to the untreated group, CD31: P<0.05, OPN: P<0.01, OCN: P<0.001.*

Gross pathology findings

The macroscopic findings on the 40th and 80th post-surgery were scored by two independent pathologists and recorded in table 6. A bone-like tissue filled the defect in the PMA-loaded scaffold and autograft groups, and the scaffold was replaced by fibrous and cartilaginous tissues in the lesions of the scaffold group [Figure 3(A)]. The lesions replaced by fibrous connective tissue in the non-treated group. The highest rate of healing was present in the PMA-loaded scaffold and autograft groups when compared to the untreated group *(P < 0.01*). However, there was no significant difference between the autograft and PMA-loaded scaffold groups (*P > 0.05*).

Group	Macroscopic Score (Day 40) Median (Min-Max)	Macroscopic Score (Day 80) Median (Min-Max)
Untreated defect (1)	0(0-0)	1(0-1)
Autograft (2)	2(2-2)	3(3-3)
Scaffold (3)	1(1-2)	2(2-3)
Scaffold + PMA (4)	2(1-2)	3(2-3)

Table 6: *Kruskal-Wallis non-parametric ANOVA, complete union (+3 score), presence of cartilage (+2 score), presence of fibrous connective tissue (+1 score), nonunion (0 score). Day 40: P<0.01 (1 vs. 2, 4); P<0.05 (1 vs. 3). Day 80: P<0.01 (1 vs. 2, 4); P<0.05 (1 vs.3).*

Radiology and CT scan findings

The radiographs revealed that a newly formed bone tissue filled the gap after 40 and 80 days post-operation [Figure 3(A)]. The differences among the control and PMA-loaded scaffold is shown in Figure 3(B) on both the 40th and 80th days post-surgery (*P < 0.001).* A significant difference existed between the scaffold and control groups on day 40 post-injury (*P < 0.05*) and on day 80 post-injury (*P < 0.01*). Also, there was no significant differences between the autograft and PMA-loaded scaffold groups after 80 days post-operation.

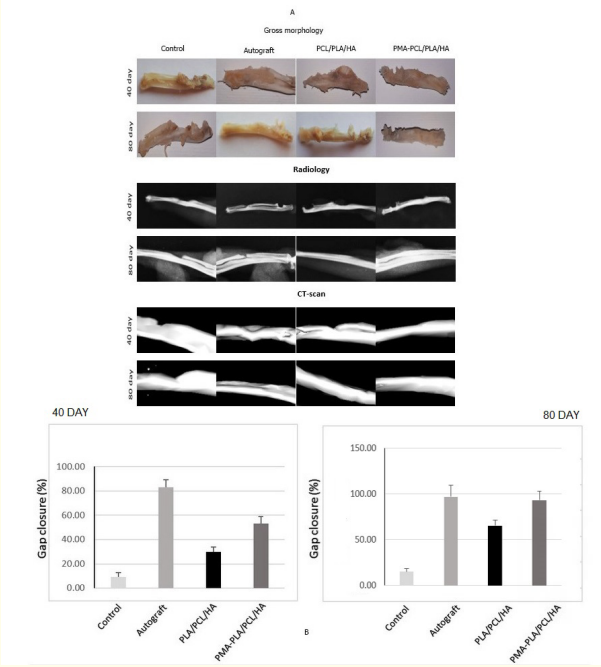

Figure3: *A: Gross morphology and radiographs imaging of the defects after 40 and 80 day post-injury (five rats were euthanized after 40¬th ¬¬ day of injury in each group, similar to the last day of investigation). The defect region of the autograft, scaffold, and PMA-PLA/PCL/HA groups were filled by hard tissues. The scaffold residues were observed in the scaffold and PMA-loaded scaffold groups on the 40th day post-injury. B: Radiographic measurements of the gap closure (%) in all groups. 40 day: Control group vs. Scaffold group P<0.05, PMA-loaded scaffold group vs. Scaffold group P<0.01, PMA-loaded scaffold group vs. Control group P<0.001. 80 day: Scaffold group vs. Control group P<0.01, PMA-loaded scaffold group vs. Control group P<0.001.*

Histopathologic and histomorphometric findings

Fibroblasts, new blood vessels, and loose areolar connective tissue were present in the lesion of the control group on the 40th day after surgery (Figure 4). The defect area of the control group was replaced by fibrous connective tissue and many newly formed blood vessels; however, fibrocartilage tissue was also present at the edges of the incised bones, on day 80 post-injury (Figure 5). Complete new bone formation filled the gap in the autograft group on the 80th days post-surgery; however, the osseous tissue noticed on the edges of the incised bones of four animals of this group, on the 40th day post-operation. Some scaffold residues that were surrounded by fibrous connective tissue were still preserved in the defect site, on day 40 post-operation, in the scaffold group. However, woven bone, cartilage, fibrocartilage, and fibrous connective tissue without any scaffold residue filled the defect region on the 80th day post-injury in this group. Although few

scaffolds residue was still present in the lesion of the PMA-loaded scaffold group, on the 40th post-operative day, the extent of woven bone was higher and the density of fibrocartilage tissue was lower in the defect area of the animals of this group in comparison to those of the scaffold group, at this time point. Compact bone, woven bone, cartilaginous and fibrocartilage tissue existed in the PMA-loaded scaffold on the 80th post-operative day and the PLA/PCL/HA scaffold was thoroughly degraded at this period.

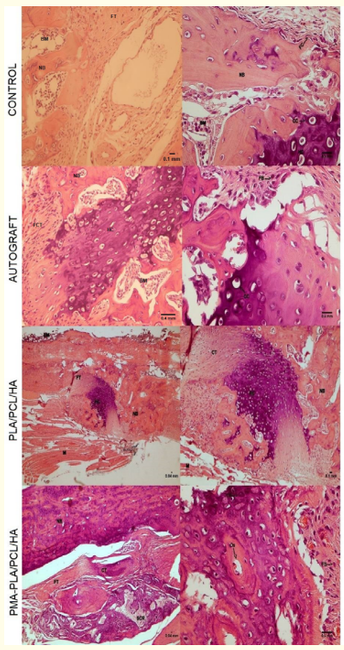

Figure 4: *Histopathological sections from the radius bone defects after 40 days post-injury. The defects in the scaffold group were filled by cartilage tissue. The defect sites in the PMA-loaded scaffold group, were filled by cartilaginous and bonny tissues. The lesions in the untreated group were filled with almost fibrous connective tissue and showed the lowest rate of healing. (BM=bone marrow, M=muscle, NB=new bone, Os=osteon, FT=fibrous tissue, CT=cartilaginous tissue, HC=hyaline cartilage, G=gap, CC=chondrocyte, FC=fibrocyte, FB=fibroblast, SCR=scaffold residue).*

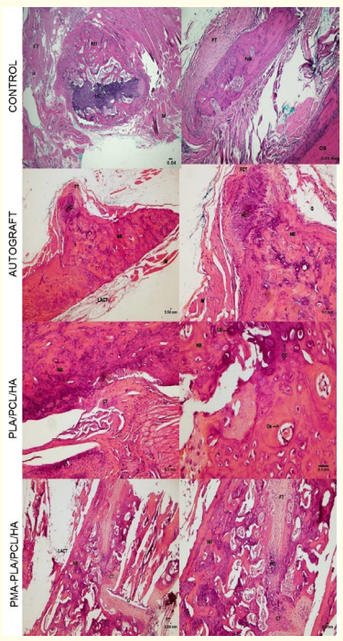

Figure 5: *Sections of the radius bone defects after 80 days post-injury. The implanted scaffold was degraded and superseded with new fibrous connective tissue, cartilage and bone tissue. The best results were observed in the autograft and PMA-loaded PCL/PLA/HA groups that the defects were absolutely replaced by new cartilage and bonny tissues. (BM=bone marrow, M=muscle, NB=new bone, Os=osteon, FT=fibrous tissue, FCT=fibrocartilaginous tissue, CT=cartilaginous tissue, HC=hyaline cartilage, OB=old bone, G=gap, CC=chondrocyte, CB=chondroblast, LACT=loose aleolar connective tissue).*

The highest density of new bone tissue referred to the autograft and PMA-loaded scaffold groups in comparison to the untreated group based on the histomorphometric results (*P < 0.05*) (Table 7). The extent of fibrous connective tissue was significantly higher in the untreated group compared to other experimental groups (*P < 0.05*), and there was a significant difference between the control and the PMA-loaded scaffold groups regarding new bone formation at the 40th and 80th days post-surgery (*P < 0.05*). The cartilage tissue was also significantly higher in the PMA-loaded scaffold, PCL/PLA/HA scaffold, and autograft groups than the defect group (*P < 0.05*).

	Mean ± SD					
Values	**FB± FC**	**CB ± CC**	**OB ± OC**	**Osteoclast**	**Osteon**	**Blood Vessels**
Control (1)	179.12 ± 22.51	8.66 ± 3.49	6.33 ± 0.85	0	0	14.66 ± 4.77
Autograft (2)	7.33 ± 3.31	27.33 ± 3.14	214.59 ± 23.66	3.12 ± 1.10	6 ± 0.84	5 ± 1.68
PLA/PCL/HA (3)	14.34 ± 4.23	21.66 ± 2.99	170.12 ± 4.44	1.22 ± 0.97	4 ± 1.68	7.33 ± 2.11
PMA- PLA/PCL/HA (4)	8.39 ± 4.5	26.10 ± 3.21	199 ± 12.68	2.98 ± 1	5.21 ± 1.34	6 ± 1.38

Table 7: *Histomorphometric Finding of the defect site after 80 day of surgery. One-way ANOVA followed by Tukey post hoc test. FB, fibroblast; FC, fibrocyte; CB, chondroblast; CC, chondrocyte; OB, osteoblast; OC, osteocyte [P<0.01 (1 vs. 2, 3, 4), P<0.05 (2 vs. 3)], SD, standard deviation.*

Immunohistochemistry observation

The IHC markers of the osteogenic and angiogenic capacity of each group are shown in figure 6. Significantly higher CD31 expression was depicted in the scaffold, PMA-loaded and autograft groups compared to the non-treated group *(P < 0.05*). A significantly lower level of angiogenic and osteogenic markers was demonstrated in the lesion of the untreated group compared to the autograft, scaffold and PMA-loaded PLA/PCL/HA groups (*P < 0.001*). Significantly lower OC expression level was depicted in the lesion of the non-treated group than the autograft, scaffold and PMA-loaded PCL/PLA/HA groups (*P < 0.05*).

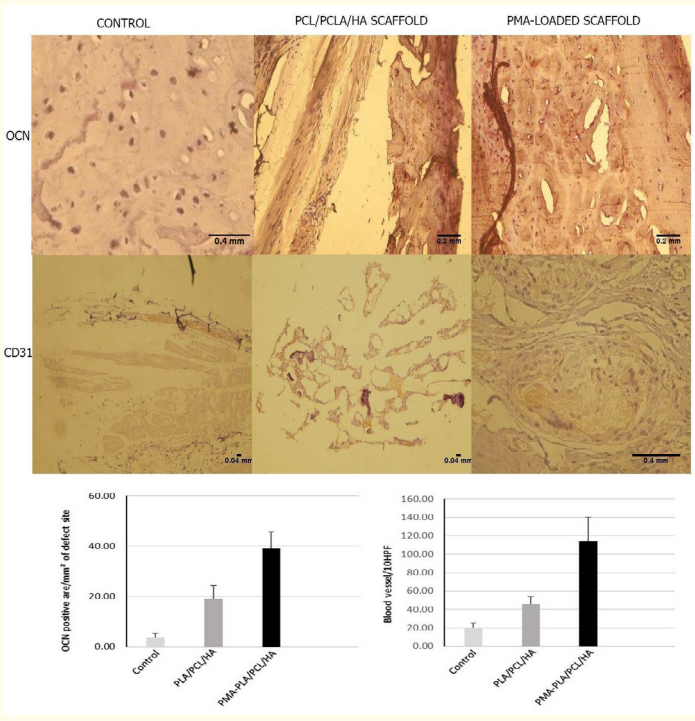

Figure 6: *IHC images of the defect area in the control, scaffold, and PMA-loaded scaffold groups based on osteogenesis and angiogenesis markers. Analysis of the CD31, and OCN genes showed the osteogenesis and angiogenesis potential of all samples. The positive staining was determines by brown color for OCN, and CD31. OCN: Scaffold group vs. Control group P<0.01, PMA-loaded scaffold group vs. Scaffold group P<0.01, PMA-loaded scaffold group vs. Control group P<0.001. CD31: Scaffold group vs. Control group P<0.05, PMA-loaded scaffold vs. Control and Scaffold groups P<0.001.*

Biomechanical findings

As it has been shown in figure 7, the PMA-loaded PLA/PCL/HA scaffold and autograft groups demonstrated significantly higher stiffness (N/mm), maximum load (N), and maximum stress (N/mm^2), in comparison to the untreated group (*P < 0.01)*. On the other hand, the PMA-loaded scaffold and the autograft groups showed significantly lower strain (%) compared to the empty defects (*P < 0.001*).

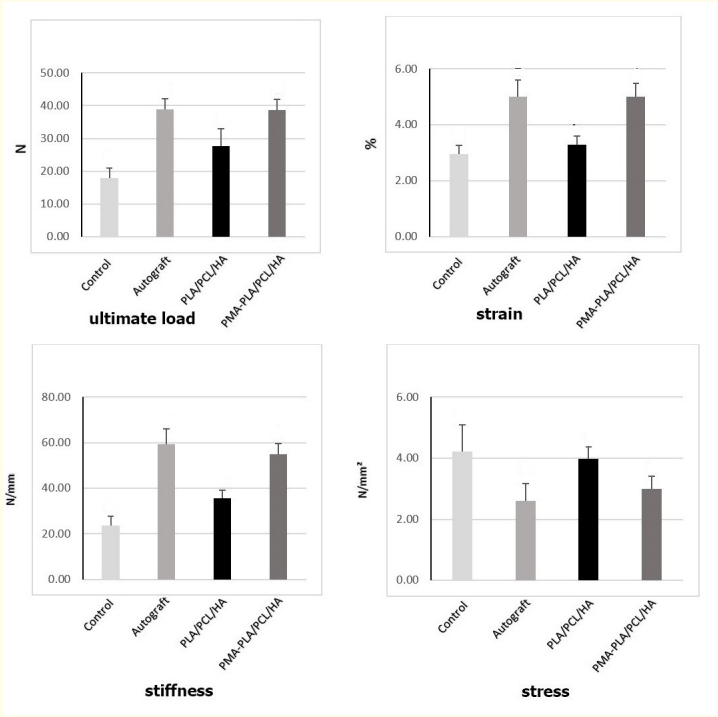

Figure 7: *Biomechanical analysis after 80 days post-surgery. Ultimate load: P<0.01 (control vs. autograft and PMA-scaffold), P<0.05 (control vs. scaffold), (scaffold vs. autograft and PMA-scaffold). Strain: P<0.001 (control vs. autograft and PMA-scaffold), P<0.01 (control vs. scaffold), (scaffold vs. autograft and PMA-scaffold). Stress: P<0.01 (control vs. autograft and PMA-scaffold), (scaffold vs. autograft and PMA-scaffold). Stiffness: P<0.001 (control vs. autograft and PMA-scaffold), P<0.01 (control vs. scaffold), (scaffold vs. autograft and PMA-scaffold).*

Discussion

A complex set of regulated signaling pathways reabsorb the damaged matrix of bone and control the new bone matrix formation, which has roles in bone repair. The primarily mediated pathway is initiated by osteoblasts to produce new bone and also by osteoclasts to resorb the bone tissue. In some cases, the catabolic and/or anabolic responses are not balanced. Such an imbalance may disrupt the healing process and end to delayed union or non-union [38].

PMA is a small biologically active molecule that accelerates the induction of the critical developmental genes' expression and is easily removed from the culture system [39,40]. In this experiment, we used the combination of hydroxyapatites (HA), polycaprolactone (PCL) and polylactic acid (PLA) to manufacture a bone implant. We aimed to compare the effect of the scaffold fabricated by an indirect 3D printing and the PMA-loaded scaffold with autograft as the golden treatment strategy of bone defects. The ability of scaffold in filling the gap with more mature compact bone tissue was estimated, and its biodegradability without causing any toxicity for the body, osteoblasts, and other osteogenic cells was also evaluated. Shahrezaee and colleagues revealed that the PCL/PLA composite was a suitable scaffold to be applied in critical bone defects due to its biocompatibility and biodegradability, but it could not provide the osteoinductivity potential and mechanical strength [41]. The fabricated scaffold in our study still had some problems with hydrophilicity and mechanical strength, which were solved by adding HA nanoparticles. The porosity of the scaffold to transfer oxygen and nutrients to result a proper environment for cells to survive and migrate was in an acceptable range. The manufactured PCL/PLA/HA scaffold had a compatible and tolerable texture with bone tissue and its mechanical performance was also suitable for bone structure.

Eshraghi and Das stated that the stoichiometric value [Ca/P = 1.7 - 1.8] in the HA particles is the best proportional rate to bone tissue [42]. The PLA/PCL/HA scaffold's compressive behavior resembled the Hassanajili., *et al.* study. They included the linear behavior (elastic response), steady stress, pores' collapse, and densification of the scaffold [43]. The results of the XRD test depicted that the crystallinity of PCL was higher than PLA and because of PLA the broadness peaks of the composite showed a reduction of PLA crystallinity. HA was responsible for the characteristic peaks and also had the peaks of both neat PCL and PLA. All these results may refer to the HA and PLA interactions. The hydrogen-bonding interactions of the HA and PLA chemical groups in the scaffold would cause the shifts of peaks of the FTIR diagram. The pH changes showed buffering behavior due to HA particles. It has been stated that the pH increase led to hinder the HA nanoparticles, which caused the impression swelling response of acidic polymer degradation [44,45]. The results of the rheology test depicted that the shear-thinning behavior with the zero shear viscosity trend was PCL > PLA/PCL (50/50) > PLA. It demonstrated that PCL increased the scaffold elasticity, so that the implant was more prominent for bone tissue. By doing all these tests on the scaffold, we concluded that the implant was proper to be applied as a bone scaffold.

Endochondral ossification was a major result of the Hh signaling pathway to make the new bone tissue by transforming the chondrocytes to make a mature bone [27]. The Hh pathway has five components (Hh ligand, transmembrane patched receptor, Smo, glioma-associated oncogene homolog transcription factors, and repressor protein complex with fused suppressor) and activation of each of them would lead to some healing processes [27]. Ultimately, this drug up-regulated different proteins which recruited for stem cell differentiation to the osteogenic cells [24,46,47]. By loading PMA with PLA/PCL/HA scaffold it promoted the osteogenic effect to obtain more efficient healing. This drug up-regulates the ALP activity to result in enhanced activity of osteoblasts because it has been shown that PMA can induce differentiation of osteoblast and promote bone-like formation [48]. It has also been shown that a dose of 3 μM PMA has an osteopromotive effect on the human-BMSCs and results in enhanced MSCs differentiation [29]. However, the osteogenic effect of PMA on the non-MSC cultures and the osteoinductive effect of this drug on human-MSCs at 2 μM dose in absence of osteogenic culture has previously been reported [23-25,30]. It has been shown that the 2 μM dosage of PMA, up-regulated PTCH1, GLI2, SMO, GLI1, BMPs and RUNX-2 after 14 days and led to osteogenesis potential to promote bone formation [25].

We designed this project based upon the differentiation capacity and the proliferation capability of PMA on different mesenchymal cells to osteogenic cells. There are a few studies on the promotive effect of this drug loaded on the 3D scaffolds. Rezia-Rad and colleagues specified that PMA enhanced proliferation and attachment and differentiated the human dental pulp stem cells to the osteogenic cells that were cultured on the β-tricalcium phosphate granules [49]. It has also been reported that secretion of ALP increased from the osteoblast-like cells when PMA was included in the 2D culture medium and the BSP, RUNX-2, OC and COL1 genes were expressed which reveal the osteoblastic differentiation potential of this drug [31,50]. In this experimental study, we stated the osteoinductivity, osteogenesis, and angiogenic potential of the PMA loaded fabricated scaffold with qRT-PCR via CD31, OCN, and OPN up-regulation. The expression of the osteoblastic marker known as OCN declared the osteogenic superiority of the PMA loaded- scaffold.

Because of the absence of an *in vivo* experiment of PMA loaded on the 3D scaffold (PLA/PCL/HA), we performed this study to understand the actual and verifiable effects of this drug with the drug delivery approach. The imaging techniques, including CT-scan and radiology were performed and it was concluded that complete union was only present in the lesions of the PMA-loaded scaffold and autograft groups on the 80th day post-treatment. The IHC results showed that the capacity of new bone and new vessel formation was significantly higher in the treated groups than the untreated ones and the highest level of bone density and angiogenesis were present in the PMA-loaded scaffold and autograft groups.

The histopathologic findings revealed that bone tissue did not develop in the untreated, but it was observed in three other groups with different maturity. The process of endochondral ossification was observed in the autograft, PMA-loaded and drug-free scaffold groups. The histopathological and histomorphometric observation revealed the most remodeled compact bone in the autograft and PMA-loaded

scaffold groups. On the other hand, the biodegradability of the scaffold was observed on both 40 and 80 days post-surgery. There was no inflammation after implanting this scaffold in the defect area on the 40th and 80th days post-injury. Thus, the PMA-loaded scaffold had a proper potential similar to the autograft as the golden treatment strategy by histopathology, IHC, and radiology tests and it seems this treatment regimen could be an acceptable substitute for autograft. It was notable that the drug-free scaffold also effectively resulted in bone regeneration and showed a significant difference with the empty defect. The SEM images of the cell-seeded scaffold showed that the cells were properly adhered to the scaffold. Further, based on the qRT-PCR results we demonstrated promotion of the osteoinductivity potential of the scaffold when it was accompanied by PMA (based upon improved expression of the osteogenic markers). In fact, our fabricated scaffold not only showed the osteoconductivity and osteoinductivity potential, but it also provided a suitable chance for the cells to migrate to various sites throughout the scaffold because of its proper porosity.

The PMA-loaded scaffold group was almost comparable and showed no significant difference with the autograft group in maximum load at 80 days post-operation. It seems the cancellous and compact bone tissue architecture developed in the PMA-loaded scaffold group enhanced the load-bearing function and resulted in improved mechanical performance in the regenerated tissue of the animals of this group [51]. Our fabricated (PLA/PCL/HA) scaffold could help healing by establishing a circumference to grow, migrate, and increase cells from the injured site at earlier stages of wound healing. Moreover, by the drug delivery system, the bone regeneration capability was enhanced and accelerated filling of the defect and resulted in improved quality of the regenerated tissue. The PMA-loaded scaffold was also a proper implant in reducing the period of regeneration. It needs more study to receive further data and knowledge regarding other drugs to be loaded on this scaffold that are useful in mesenchymal cell proliferation, differentiation and migration to initiate bone tissue regeneration.

Conclusion

The PLA/PCL/HA scaffold was a reliable bone implant both *in vitro* and *in vivo* conditions. Loading this scaffold by PMA enhanced cell differentiation of the stem cells to the osteogenic precursor cells. The scaffold surface was also suitable for cells to differentiate and migrate. Thus, the results of this investigation showed the osteoinductivity of the scaffold, which was improved by loading PMA onto it.

Animal Right Statement

The experimental protocols were performed according to the Guide for Care and Use of Laboratory Animals published by the National Institutes of Health (NIH publication No. 85-23). Additionally, the local Ethics Committee of "Regulations for using animals in scientific procedures" in School of Veterinary Medicine of our university approved this experiment.

Acknowledgement

Our study was supported by Veterinary School, Shiraz University, Shiraz, Iran. The authors would also thank the INSF (grant number 96006039) for partial financial support.

Conflict of Interests

There is no conflict.

Author Contribution

The hypotheses and experimental designs were stated by AO and SH. AO and SS carried out experiments and completed computational analysis. All authors discussed the results and reviewed the final manuscript.

Declaration of Interest

Not applicable.

Bibliography

1. Oryan A., *et al*. "Bone regenerative medicine: Classic options, novel strategies, and future directions". *Journal of Orthopaedic Surgery and Research* 9 (2014): 18.

2. Oryan A., *et al*. "Effects of osteogenic medium on healing of the experimental critical bone defect in a rabbit model". *Bone* 63 (2014): 53-60.

3. Moshiri A., *et al*. "An overview on bone tissue engineering and regenerative medicine: current challenges, future directions and strategies". *Journal of Sports Medicine and Doping* Studies 5 (2015): e144.

4. Alidadi S., *et al*. "Comparative study on the healing potential of chitosan, polymethylmethacrylateand demineralized bone matrix in radial bone defects of rat". *Carbohydrate Polymers* 166 (2017): 236-248.

5. Cheng H., *et al*. "Development of nanomaterials for bone-targeted drug delivery". *Drug Discovery Today* 22 (2017): 1336-1350.

6. Mathavan N., *et al*. "Investigating the synergistic efficacy of BMP-7 and zoledronate on bone allografts using an open rat osteotomy model". *Bone* 56 (2013): 440-448.

7. Kyllonen L., *et al*. "Local drug delivery for enhancing fracture healing in osteoporotic bone". *Acta Biomaterialia* 11 (2015): 412-434.

8. Stevens MM. "Biomaterials for bone tissue engineering". *Mater Today* 11 (2008): 18-25.

9. Peter M., *et al*. "Protein growth factors loaded highly porous chitosan scaffold: a comparison of bone healing properties". *Chemical Engineering* 158 (2010): 353-361.

10. Croisier F and Jerome C. "Chitosan-based biomaterials for tissue engineering". *European Polymer Journal* 49(2013): 780-792.

11. Oryan A., *et al*. "Effectiveness of tissue engineered chitosan-gelatin composite scaffold loaded with human platelet gel in regeneration of critical sized radial bone defect in rat". *Journal of Controlled Release* 254 (2017): 65-74.

12. Moshiri A., *et al*. "Role of tissue-engineered artificial tendon in healing of a large achilles tendon defect model in rabbits". *College of Surgeons* 217 (2013): 421-441.

13. Rodríguez-Vazquez M., *et al*. "Chitosan and its potential use as a scaffold for tissue engineering in regenerative medicine". *BioMed Research International* 2015 (2015): 821279.

14. Oryan A., *et al*. "Comparative study on the role of gelatin, chitosan and their combination as tissue engineered scaffolds on healing and regeneration of critical sized bone defects: an in vivo study". *Journal of Materials Science: Materials in Electronics* 27 (2016): 155.

15. Shahrezaie M., *et al*. "Effectiveness of tissue engineered three-dimensional bioactive graft on bone healing and regeneration: an in vivo study with significant clinical value". *Journal of Tissue Engineering and Regenerative Medicine* 12 (2017): 936-960.

16. Wang W and Yeung KWK. "Bone grafts and biomaterials substitutes for bone defect repair: A review". *Bioactive Materials* 2 (2017): 224-247.

17. Witzler M, *et al*. "Non-cytotoxic agarose/hydroxyapatite composite scaffolds for drug release". *International Journal of Molecular Sciences* 20 (2019): 35-65.

18. Zhang ZZ., *et al*. "3D printed poly(ε-caprolactone): scaffolds function with simvastatin-loaded poly (lactic-co-glycolic acid): microspheres to repair load-bearing segmental bone defects". *Experimental and Therapeutic Medicine* 17 (2019): 79-90.

19. Xu T., *et al*. "Tailoring weight ratio of PCL/PLA in electrospun three-dimensional nanofibrous scaffolds and the effect on osteogenic differentiation of stem cells". *Colloid Surfaces B* 171 (2018): 31-39.

20. Rodenas-Rochina J., *et al*. "Effects of hydroxyapatite filler on long-term hydrolytic degradation of PLLA/PCL porous scaffolds". *Polymer Degradation and Stability* 119 (2015): 121-131.

21. Eftekhari H., *et al*. "Histopathological evaluation of polycaprolactone nanocomposite compared with tricalcium phosphate in bone healing". *Veterinary Research* 62 (2018): 385-394.

22. Kumar P., *et al*. "Bioceramics for Hard Tissue Engineering Applications: A Review". *International Journal of Applied Engineering Research* 13 (2018): 2744-2752.

23. Wu X., *et al*. "Small molecule with osteogenesis-inducing activity in multipotent mesenchymal progenitor cell". *Journal of the American Chemical Society* 124 (2002): 14520-14521.

24. Wu X., *et al*. "Purmorphamine induces osteogenesis by activation of the hedgehog signaling pathway". *ACS Chemical Biology* 11 (2004): 1229-1238.

25. Oliveira FS., *et al*. "Hedgehog signaling and osteoblast gene expression are regulated by purmorphamine in human mesenchymal stem cells". *Journal of Cellular Biochemistry* 113 (2012): 204-208.

26. Sinha S and Chen JK. "Purmorphamine activates the hedgehog pathway by targeting smoothened". *Nature Chemical Biology* 2 (2006): 29-30.

27. Aravamudhan A., *et al*. "Osteoinductive small molecules: growth factor alternatives for bone tissue engineering". *Current Pharmaceutical Design* 19 (2013): 3420-3428.

28. Plaisant M., *et al*. "Activation of hedgehog signaling inhibits osteoblast differentiation of human mesenchymal stem cells". *Stem Cell* 27 (2009): 703-713.

29. Faghihi F., *et al*. "The effect of purmorphamine and sirolimus on osteogenic differentiation of human bone marrow-derived mesenchymal stem cells". *Biomed Pharm* 67 (2013): 31-38.

30. Beloti MM., *et al*. "Purmorphamine enhances osteogenic activity of human osteoblasts derived from bone marrow mesenchymal cells". *Cell Biology International* 29 (2005): 537-541.

31. Bahrami N., *et al*. "The effect of purmorphamine on differentiation of endometrial stem cells into osteoblast-like cells on collagen/hydroxyapatite scaffolds". *Artificial Cells, Nanomedicine, and Biotechnology* 45 (2017): 1343-1349.

32. Ostafinska A., *et al*. "Synergistic effects in mechanical properties of PLA/PCL blends with optimized xomposition, processing, and morphology". *RSC Advances* 5 (2015): 98971-98982.

33. Mou ZL., *et al*. "Preparation of porous PLGA/HA/collagen scaffolds with supercritical CO2 and application in osteoblast cell culture". *The Journal of Supercritical Fluids* 58 (2011): 398-406.

34. Raucci MG., *et al*. "Hybrid composite scaffolds prepared by sol-gel method for bone regeneration". *Composites Science and Technology* 70 (2010): 1861-1868.

35. Bassi A., *et al*. "The chemical and physical properties of poly(ε-caprolactone): scaffolds functionalised with poly (vinyl phosphonic acid-co-acrylic acid)". *Journal of Tissue Engineering* 2011 (2011): 615328.

36. Oryan A., *et al*. "Synergistic effect of strontium, bioactive glass and nano-hydroxyapatite promotes bone regeneration of critical-sized radial bone defects". *Journal of Biomedical Materials Research Part B* 107(2018): 50-64.

37. Oryan A and Alidadi S. "Reconstruction of radial bone defect in rat by calcium silicate biomaterials". *Life Sciences* 201 (2018): 45-53.

38. Doi Y., *et al*. "Manipulation of the anabolic and catabolic responses with BMP-2 and zoledronic acid in a rat femoral fracture model". *Bone* 49 (2011): 777-782.

39. Andrews PD. "Discovering small molecules to control stem cell fate". *Future Medicinal Chemistry* 3 (2011): 1539-1549.

40. Spring DR. "Chemical genetics to chemical genomics: small molecules offer big insights". *Chemical Society Reviews* 34 (2011): 472-482.

41. Shahrezaee M., *et al*. "In vitro and in vivo investigation of PLA/PCL scaffold coated with metformin-loaded gelatin nanocarriers in regeneration of critical sized bone defects". *Nanomedicine* 14 (2018): 2061-2073.

42. Eshraghi S. and Das S. "Micromechanical finite element modeling and experimental characterization of the compressive mechanical properties of polycaprolactone: hydroxyapatite composite scaffolds prepared by selective laser sintering for bone tissue engineering". *Acta Biomater* 8 (2012): 3138-3143.

43. Hassanajili S., *et al*. "Preparation and characterization of PLA/PCL/HA composite scaffolds using indirect 3D printing for bone tissue engineering". *Materials Science and Engineering C* 104(2019): 1099960.

44. Misra SK., *et al*. "Effect of nanoparticulate bioactive glass particles on bioactivity and cytocompatibility of poly(3-hydroxybutyrate): composites". *Journal of the Royal Society Interface* 7 (2009): 453-465.

45. Roohani-Esfahani S., *et al*. "Effects of bioactive glass nanoparticles on the mechanical and biological behavior of composite coated scaffolds". *Acta Biomater* 7 (2011): 1307-1318.

46. Bijlsma MF., *et al*. "Hedgehog morphogen in cardiovascular disease". *Circulation* 114 (2006): 1985-1991.

47. Briscoe J. "Agonizing hedgehog". *Nature Chemical Biology* 2 (2006): 10-11.

48. Kim YH. and Tabata Y. "Dual-controlled release system of drugs for bone regeneration". *Advanced Drug Delivery Reviews* 94 (2015): 28-40.

49. Rezia-Rad M., *et al*. "Purmorphamine increased adhesion, proliferation and expression of osteoblast phenotype markers of human dental pulp stem cells cultured on beta-tricalcium phosphate". *Biomed Pharma* 82 (2016): 432-438.

50. Arpornmaeklong P., *et al*. "Expansion and characterization of human embryonic stem cell-derived osteoblast-like cells". *Cellular Reprogramming* 12 (2010): 377-389.

51. Henkel J., *et al*. "Bone regeneration based on tissue engineering conceptions-A 21st century perspective". *Bone Research* 1 (2013): 216-248.

Volume 13 Issue 6 June 2022